Thermal-Hydraulic Analyses Of The LS-VHTR

ICAPP '06

Cliff B. Davis
Grant L. Hawkes

June 2006

Idaho National Laboratory

Thermal-Hydraulic Analyses of the LS-VHTR

Cliff B. Davis and Grant L. Hawkes
Idaho National Laboratory
P.O. Box 1625
Idaho Falls, ID 83415-3890
Tel: 208 526 9470 , Fax: 208 526 0528 , Email: Cliff.Davis@inl.gov

Abstract – Thermal-hydraulic analyses were performed to evaluate the safety characteristics of the Liquid-Salt-Cooled Very High-Temperature Reactor (LS-VHTR). A one-dimensional model of the LS-VHTR was developed using the RELAP5-3D computer program. The thermal calculations from the one-dimensional model of a fuel block were benchmarked against a multi-dimensional finite element model. The RELAP5-3D model was used to simulate a transient initiated by loss of forced convection in which the Reactor Vessel Auxiliary Cooling System (RVACS) passively removed decay heat. Parametric calculations were performed to investigate the effects of various parameters, including bypass flow fraction, coolant channel diameter, and the coolant outlet temperature. Additional parametric calculations investigated the effects of an enhanced RVACS design, failure to scram, and radial/axial conduction in the core.

I. INTRODUCTION

Thermal-hydraulic analyses were performed to evaluate the safety characteristics of the Liquid-Salt-Cooled Very High-Temperature Reactor (LS-VHTR). The LS-VHTR has been proposed[1] to address a growing interest in developing nuclear systems capable of generating electricity with much higher efficiency than current plants and additionally capable of large-scale production of hydrogen.

The LS-VHTR represents a unique merging of design features from other reactor systems. The reactor core is similar to that used in graphite-moderated helium cooled reactor systems, such as Fort St. Vrain and the Gas-Turbine Modular High-Temperature Reactor. The LS-VHTR uses the same coated particle fuel, cylindrical fuel compacts, and hexagonal graphite fuel assemblies as these reactors. The liquid salt coolant allows for efficient heat transfer and is based on experience gained from the earlier Molten Salt Reactor program. Because the liquid salt coolant operates at low pressure, the vessel enclosure system and facility design are similar to pool-type sodium reactors. The passive decay heat removal system is based on the Power Reactor Inherently Safe Module (PRISM) developed by General Electric.

A one-dimensional model of the LS-VHTR was developed using the RELAP5-3D computer program.[2] The program was originally developed for thermal-hydraulic analysis of light water reactors and related experimental systems during loss-of-coolant accidents and operational transients. The code has recently been improved to simulate candidate Generation IV designs cooled by gas,[3] supercritical water,[4] and lead-bismuth.[5] Liquid salt coolants have also been implemented into the code,[6] which allows it to simulate the LS-VHTR. The primary coolant was assumed to be Flibe, which consists of LiF-BeF_2 in a molar mixture that is 66% LiF and 34% BeF_2, for this analysis.

The thermal calculations from the one-dimensional model of a fuel block were benchmarked against a multi-dimensional ABAQUS[7] model. The RELAP5-3D model was then used to simulate a transient initiated by loss of forced convection in which the Reactor Vessel Auxiliary Cooling System (RVACS) passively removed decay heat. Parametric calculations were performed to investigate the effects of various parameters, including bypass flow fraction, coolant channel diameter, and the coolant outlet temperature. Additional parametric calculations investigated the effects of an enhanced RVACS design, failure to scram, and radial/axial conduction in the core.

II. MODEL DESCRIPTION

The RELAP5-3D model of the LS-VHTR is illustrated in Fig. 1. The model represents the portion of the primary coolant system within the reactor vessel and the RVACS. The primary coolant is represented by Components 120 through 290. The inlet plenum is represented by Components 120 through 140. The core is represented by Components 151 through 156. The ten fueled rings in the design are simulated with six channels in the model. The inner two high-powered rings are modeled explicitly with Components 151 and 152. The remaining eight rings are represented with four channels (Components 153 through 156), each of which represents two rings in the design. The outer eight rings were combined into four channels so that the effects of radial and axial conduction between prismatic blocks in the core could be simulated. Parametric calculations to be discussed later showed that the effects of conduction between blocks were small in the LS-VHTR. Consequently, each fueled ring could be modeled explicitly to better characterize the radial temperature profile if desired. Each of the core channels is modeled with 12 axial control volumes. The upper and lower control volumes represent the axial reflectors. The other ten volumes represent the active core region.
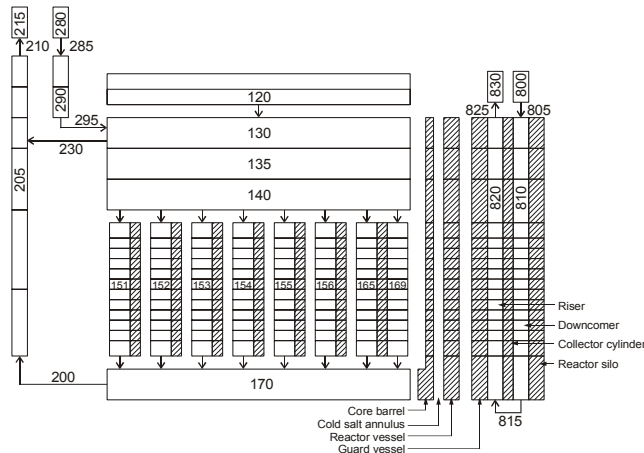

Fig. 1. RELAP5-3D model of the LS-VHTR.

The outlet plenum is modeled with Component 170. Component 290 simulates the inlet lines to the reactor vessel while Component 205 simulates the coolant risers, which connect the outlet plenum and the heat exchangers. The heat exchangers and pumps are not modeled explicitly, but their effects are modeled with boundary conditions of flow in Component 285, temperature in Component 280, and pressure in Component 215. The flow area of the coolant risers is based on that of eight hexagonal blocks in the outer reflector.

The model simulates a thermal blanket system that consists of a core barrel and an annulus filled with cold salt. The thickness of the annulus was set to limit the reactor vessel temperature in the inlet plenum to 750 °C during normal operation, assuming that conduction was the only heat transport mechanism through the salt. Additional insulation, assumed to be graphite, was required to limit the reactor vessel temperature near the outlet plenum, which was 100 °C hotter than the inlet plenum. An engineered bypass path (Component 169) was used to heat the reactor vessel to near 750 °C in the core region. The engineered bypass path consists of a small gap between the outer reflector and the core barrel. Two other bypass paths around the core are represented. These bypass paths include the gaps between the fuel and reflector blocks (Component 165) and a siphon breaker between the inlet plenum and the coolant riser (Component 230).

Heat structures are used to represent the core barrel, the reactor vessel, and the prismatic blocks in the core and the upper, lower, and outer reflectors. The maximum radial power peaking factor is 1.41 and occurs in the innermost ring (Component 151). Component 155, which represents the seventh and eighth fueled rings, approximates an average channel as it has a radial power peaking factor of 0.98. The axial power profile is based on the profile used for the gas-cooled Next Generation Nuclear Plant (NGNP).[8] The axial power profile is bottom skewed, with a peak value of 1.38. The use of a bottom skewed power profile results in higher fuel temperatures than a symmetric power profile with the same peak value because the power is shifted towards the bottom of the core where the coolant temperatures are higher.

The thermal conductivity of the graphite in the prismatic blocks accounts for the effects of irradiation.[9] Irradiation initially causes a large decrease in the thermal conductivity, but the effects of continued irradiation disappear after the fast fluence exceeds $3x10^{25}$ n/m^2. The thermal conductivity used in the RELAP5-3D model applies to a radial orientation of H-451 graphite after a fast fluence of $10x10^{25}$ n/m^2. This fluence corresponds to an end-of-life (or beyond) irradiation and results in a thermal conductivity near 40 W/m-K whereas the value for unirradiated graphite is near 60 W/m-K.

The reactor power is calculated with a point kinetics model. The decay heat is calculated from the ANS-5.1 standard[10] for the infinite operation of U-235. The decay heat curve used here is about 5% higher than obtained from detailed calculations performed for the gas-cooled NGNP.

The RVACS is represented by Components 800 through 830. The air supply and exhaust are represented

with two time-dependent volumes, Components 800 and 830, that are set at atmospheric pressure. The RVACS downcomer and riser are represented by Components 810 and 820, respectively. The model represents all the major heat structures associated with the RVACS, including the reactor and guard vessels and the collector cylinder that separates the downcomer and the riser. Radiation enclosure models are used to represent the heat transfer between the reactor and guard vessels and between the guard vessel and the collector cylinder. The emissivity of these surfaces was set to 0.75, which is representative of the average measured value during the PRISM test program.[11] The convection and conduction of the inert gas in the gap between the reactor and guard vessels was neglected. The outside surface of the collector cylinder was insulated to prevent preheating of the cold air flowing down the downcomer.

The RVACS model is based on the PRISM design.[12] In the PRISM design, the hot and cold air columns were significantly longer than the length of the reactor vessel. However, details of the inlet and outlet air ducts were not provided. These inlet and outlet air ducts were neglected to simplify the model. The model was adjusted to represent RVACS performance during emergency operation in PRISM. Adjustments included setting the form loss coefficient at the bottom of the downcomer (Component 815) to 0.26 and reducing the heat transfer coefficient on the outer surface of the guard vessel and the inner surface of the collector cylinder by 20% using a fouling factor. The resulting model predicted the mass flow rate of air and the total power removed during emergency operation within 10% of the values reported for PRISM. The model of the reactor vessel was then modified to represent the LS-VHTR by increasing the diameter, thickness and height of the vessel. The changes to the reactor vessel also affected the other RVACS components, including the guard vessel, riser, collector cylinder, and the downcomer. The thicknesses of these components were based on the PRISM values.

The geometry RELAP5-3D model of the LS-VHTR is summarized in Table I.

TABLE I

Geometrical Parameters of the LS-VHTR model.

Parameter	Value
Core:	
Coolant channel diameter, mm	9.53
Fuel compact diameter, mm	12.45
Fuel channel diameter, mm	12.70
Fuel channel pitch, mm	18.8
Number of coolant channels per block	108
Number of fuel channels per block	216
Number of fuel columns	265
Flat-to-flat distance of hexagonal block, mm	360
Gap between hexagonal blocks, mm	1
Heated length, m	7.93
Length of upper and lower reflectors, m	1.19
Thickness of outer reflector, m	0.834
Thermal blanket system:	
Gap between outer reflector and core barrel, mm	5
Core barrel inner diameter, m	7.952
Core barrel thickness, mm	25
Cold salt annulus thickness, mm	9
Outlet plenum graphite insulation thickness, mm	180
RVACS:	
Reactor vessel inner diameter, m	8.02
Reactor vessel thickness, m	0.10
Gap between reactor and guard vessels, m	0.20
Guard vessel thickness, m	0.025
Riser gap thickness, m	0.178
Collector cylinder thickness, m	0.0254
Collector cylinder insulation thickness, m	0.0508
Active heat transfer length, m	18.4

The RELAP5-3D model was used to determine the steady-state operating conditions for the LS-VHTR. The results of the steady-state calculation are presented in Table II. Note that the maximum fuel temperature exceeds the proposed steady-state limit of 1250 °C. Subsequent calculations were performed with a reduced core inlet fluid temperature and larger coolant holes to identify changes that would allow the design to meet the steady-state temperature limit.

TABLE II

Initial conditions for the LS-VHTR at rated power.

Parameter	Value
Core power, MW	2400
Mass flow rate, kg/s	10,264
Core inlet temperature, °C	900
Core outlet temperature, °C	1000
Average fuel temperature, °C	1093
Maximum fuel temperature, °C	1329
Maximum RV temperature, °C	750
Total bypass, %	12.0
Gaps between blocks, %	4.4
Engineered bypass, %	5.6
Siphon breaker, %	2.0
Core pressure drop, MPa	0.211
Vessel pressure drop, MPa	0.276
RVACS heat removal, MW	6.2

III. STEADY-STATE THERMAL ANALYSIS

The RELAP5-3D model of the fuel block is based on a one-dimensional representation of a unit cell. Figure 2 shows a unit cell, which contains one coolant channel, 120° segments from the six surrounding fuel channels, and the intermediate graphite matrix. The unit cell effectively contains one coolant channel and two fuel channels. The gap between the fuel channel and the fuel compact was assumed to be filled with helium. The corresponding one-dimensional heat structure utilized annular geometry as shown in the figure. The inner radius of the heat structure was set to the radius of the coolant channel. The thickness of the graphite ring preserved the volume of the graphite. Similarly, the thicknesses of the helium and fuel rings preserved the volume of the corresponding regions in the unit cell. An additional annular region was modeled outside the fuel region to account for the graphite not contained within any unit cell, such as that near the periphery of the block.
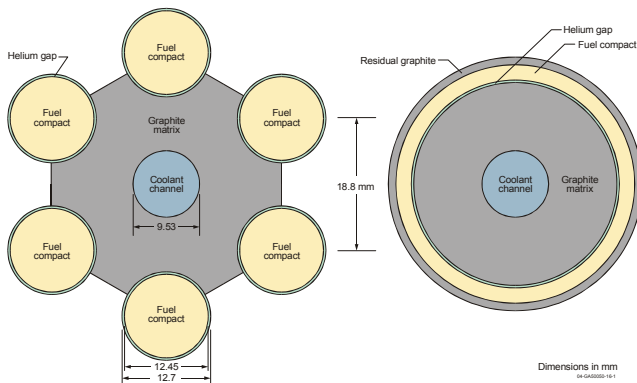

Fig. 2. RELAP5-3D model of a unit cell in a fuel block.

The annular model used here resulted in a fuel ring that was significantly smaller than the radius of the fuel compact. The thermal conductivity of the fuel was multiplied by a factor of 0.324 in the one-dimensional model to compensate for the smaller thickness. This factor was obtained from a comparison of the exact solution for the temperature rise across a cylinder with the exact solution for the temperature rise across an annulus with an outer adiabatic surface. The exact solutions utilized uniform volumetric heat generation rates and constant thermal conductivities. The use of the annular geometry also resulted in a thinner helium gap and more heat transfer area in the gap than in the actual design. The thermal conductivity of the helium was multiplied by a factor of 0.742 in the one-dimensional model to compensate for the distortion in geometry. This factor was obtained from a comparison of the exact solutions for the temperature rise across the helium gap in the fuel channel and in the one-dimensional model assuming constant thermal conductivity.

Detailed finite element calculations were performed with the ABAQUS computer code to benchmark the results obtained from the one-dimensional RELAP5-3D model. The ABAQUS model represented a 60° segment of the unit cell shown in Fig. 2. The helium gap was modeled as a heat conducting region. Convection and radiation were neglected. The ABAQUS model represented the outlet of an average-powered fuel column in last year's design of the LS-VHTR.[13] To accomplish this, the heat transfer coefficient and fluid sink temperature were set at 13,000 W/m^2-K and 1000 °C, respectively. The thermal conductivities of the graphite, helium, and fuel compact were 60, 0.44, and 10 W/m-K, respectively. The thermal conductivity of the graphite corresponds to the value used in last year's design calculations. A uniform volumetric heat generation rate in the fuel compact of 44.28 MW/m^3 was applied. A RELAP5-3D model simulating these same parameters was developed for comparison. The RELAP5-3D results presented elsewhere in this paper were generated using temperature-dependent thermal properties.

Figure 3 compares the temperatures in the unit cell calculated with RELAP5-3D and ABAQUS. The abscissa of the figure corresponds to a straight line connecting the center of the coolant and fuel channels. The increase in temperature near 4.8 mm corresponds to the thermal resistance associated with the heat transfer coefficient at the surface of the coolant channel. The temperature rise near 12.5 mm in the ABAQUS calculation and near 14.7 mm in the RELAP5-3D calculation corresponds to the thermal resistance of the helium gap. The temperature rises between the fluid and the wall, across the graphite, and across the fuel compact were nearly the same in both calculations. The centerline fuel temperature calculated by

RELAP5-3D was 1.3 °C higher than the corresponding value calculated by ABAQUS. Additional calculations were performed in which the volumetric heat generation rate was varied between 20.27 and 82.29 MW/m^3, corresponding to the minimum and maximum power locations during normal operation with this year's design. The fuel centerline temperatures calculated by RELAP5-3D were within 0.6 and 2.2 °C, respectively, of the values calculated by ABAQUS. Thus, the RELAP5-3D one-dimensional annular model can accurately predict fuel centerline temperatures given the correct thermal properties.
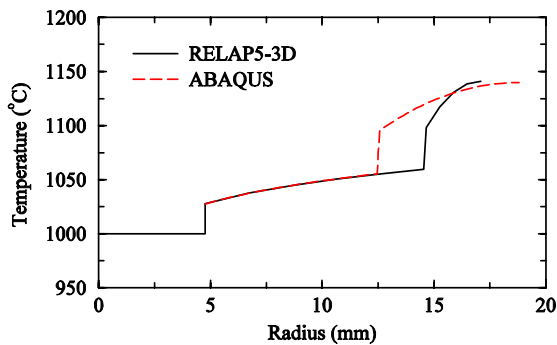

Fig. 3. A comparison of calculated temperatures in a unit cell of a fuel block.

IV. TRANSIENT ANALYSES

The RELAP5-3D model was used to simulate a transient initiated by loss of forced convection. The transient was simulated by linearly reducing the flow in Component 285 to zero in 10 s. The reactor scram signal occurred at 1 s and the control rods were fully inserted 3 s later, shutting down the reactor. RVACS was assumed to be the only system available to remove decay heat.

This transient was governed by the balance between the decay heat generated in the core and the power removed by RVACS. The dominant heat transport processes were due to natural circulation of the liquid salt within the reactor vessel, conduction through the reactor vessel, radiation between the reactor and guard vessels and the collector cylinder, and then convection from the surfaces of the guard vessel and collector cylinder to the air flowing through the riser of RVACS. Figure 4 shows that the decay heat initially exceeded the power removed by RVACS. This imbalance in power generation and removal caused the LS-VHTR to heat up, which increased the heat removal by RVACS, partially due to the increased temperature difference between the reactor and the heat sink and partially due to more effective radiation at increased temperatures. The increased heat removed by RVACS exceeded the core decay power after 61 hours, which resulted in a general cooling of the LS-VHTR.
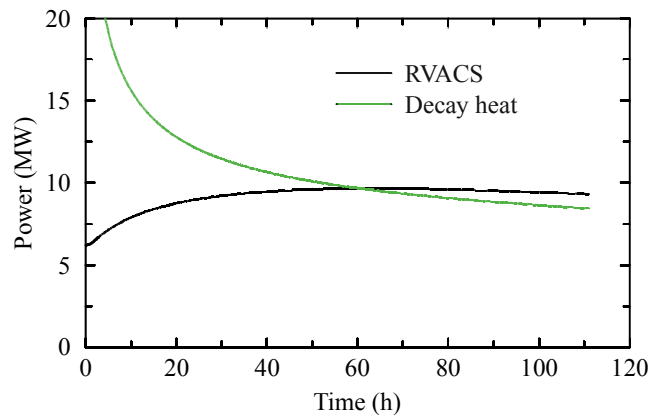

Fig. 4. A comparison of RVACS heat removal and core decay power following a loss of forced convection.

The effects of the loss of forced convection on the maximum fuel temperature in the core are shown in Fig. 5. The reactor scram caused the maximum fuel temperature to decrease sharply. The fuel temperature then increased following a flow reversal in the core and the transition to natural circulation. The reservoir of cold liquid in the inlet plenum was able to moderate the temperature increase for a few hours. However, the supply of cold liquid was eventually exhausted and the temperature increased due to the imbalance between the power generated in the core and that removed by RVACS. The peak fuel temperature was 1260 °C, and occurred near the time that the power removed by RVACS exceeded the decay power. The peak fuel temperature remained well below the boiling limit of 1430 °C for Flibe at atmospheric pressure.
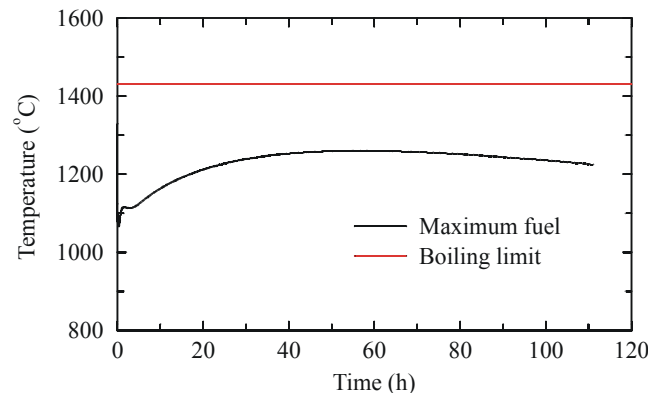

Fig. 5. Maximum fuel temperature following a loss of forced convection.

The thermal performance of the LS-VHTR is further illustrated in Fig. 6. The fluid temperature in the outlet plenum, which supplied liquid to the core after the transition to natural circulation, was generally within 100 °C of the maximum fuel temperature. Thus, the axial

temperature gradient within the vessel was relatively small, which demonstrates the effectiveness of the natural circulation as a heat transport mechanism. The radial temperature gradient in the core was also relatively small after scram. For example, the differences between fluid and centerline fuel temperatures were generally less than 6 °C after scram.
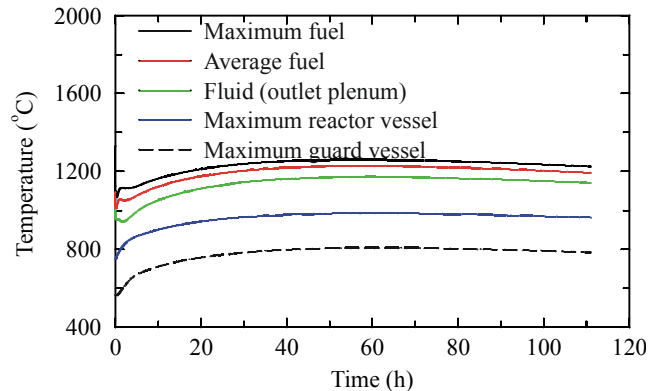

Fig. 6. Thermal performance following a loss of forced convection.

The flow patterns within the reactor vessel were fully developed about an hour after the start of the transient. Thereafter, the flow through each of the core channels was upwards. The magnitude of the velocity was consistent with the power distribution, with the highest velocity occurring in the central channel. The principal paths for downward flow were through the engineered bypass path and the coolant riser pipes, which received flow from the siphon breakers.

Analysis of the calculated results showed that radiation heat transfer between the reactor and guard vessels is more effective than conduction through liquid salt. The equivalent thermal conductivity for radiation across the 20-cm gap varies from about 20 to 40 W/m-K whereas the thermal conductivity of Flibe is only 1.1 W/m-K. Thus, a leak from the reactor vessel could cause the gap to fill with salt, which would significantly degrade the performance of the RVACS if conduction through the salt is the only heat transport mechanism. Evaluations of enclosure heat transfer correlations[14] suggest that convection in liquid salt will not be a significant heat transport mechanism between the reactor and guard vessels, but these evaluations are not definitive because the geometry of the RVACS is well outside the database of the correlations. Although data from the aluminum smelting industry suggest that other heat transfer mechanisms, such as radiation, may be important with liquid salt, the viability of the RVACS for passive cooling of the LS-VHTR in the presence of a leak cannot be assured without relevant experiments or more detailed calculations. Reference 12

evaluated the effectiveness of the PRISM RVACS with a leak from the reactor vessel. In PRISM, the effectiveness of the RVACS improved with a leak because of the high thermal conductivity of sodium, about 60 W/m-K. Note that if convection and/or radiation are effective heat transport mechanisms in the LS-VHTR RVACS, the cold salt annulus of the thermal blanket system will not be as effective as assumed here and additional insulation will be required.

Calculations were performed to investigate the sensitivity of the calculated results to various parameters, including the size of the coolant channels, the bypass flow fraction, the number of fueled rings in the core, and the coolant outlet temperature. Additional parametric calculations investigated the effects of an enhanced RVACS design, failure to scram, and radial/axial conduction in the core. In each case, the calculation was identical to the base calculation described previously except for the identified change. The results of these parametric calculations are described below.

The diameter of the coolant channel was 9.53 mm in the base calculation. Parametric calculations were performed in which the diameter was increased to 11.8 and 14.0 mm. The effects of the coolant channel diameter on the performance of the LS-VHTR are summarized in Table III. The maximum fuel temperature decreased as the channel diameter increased, primarily because of the smaller conduction distance across the graphite. The effect was modest (< 25 °C) at steady state, where the heat fluxes were relatively large, and small (< 5 °C) during the transient, where the heat fluxes were relatively small. The diameter had a large effect on the differential pressure across the vessel during normal operation. For example, the differential pressure was reduced by more than 60% with the largest diameter. A corresponding reduction would occur in the required pumping power. The reduction in differential pressure associated with the larger coolant diameter also significantly reduced the bypass flow around the core. The parametric calculations show that the thermal-hydraulic performance of the design is improved with larger coolant channel diameters.

TABLE III

The effect of coolant channel diameter on LS-VHTR performance.

Parameter	9.53 mm	11.8 mm	14.0 mm
Max. fuel temperature: Steady state / transient, °C	1329 / 1260	1312 / 1257	1304 / 1255
Vessel differential pressure, MPa	0.276	0.146	0.102
Total bypass, %	12.0	6.6	4.2

A parametric calculation was performed to determine the effect of bypass on the performance of the LS-VHTR. In the base calculation, the bypass through the gaps between the fuel and reflector columns was based on mechanistic estimates of the flow area and hydraulic diameter at cold conditions. In the parametric calculation, the hydraulic diameter of the gaps was arbitrarily increased by a factor of five. As a result, the bypass flow around the core increased to 18.3% of the total, with 11.2% of the flow passing through the gaps. The additional bypass flow reduced the flow through the coolant channels and increased the maximum fuel temperature by 12 °C at steady state. However, the increased bypass flow did not significantly affect the response of the LS-VHTR following a loss of forced convection. The maximum fuel temperature following the reactor scram increased by less than 1 °C from that shown previously.

A parametric calculation was performed to investigate the effects of coolant temperature on the performance of the LS-VHTR. The coolant inlet and outlet temperatures were reduced by 250 °C from the values shown in Table II, with resulting values of 650 and 750 °C, respectively. The 250 °C reduction in coolant temperature reduced the average and maximum fuel temperatures by 229 and 215 °C, respectively, at steady state. The reduction in fuel temperatures was less than the change in coolant temperatures because the thermal conductivities of the graphite, helium, and fuel compact increase with temperature. The heat transfer coefficient also increases with temperature because of the changes in the coolant viscosity. The maximum fuel temperature was 1114 °C, well below the steady-state limit of 1250 °C. The maximum reactor vessel temperature was reduced by 161 °C to 589 °C.

The effect of the initial coolant temperature on the power removed by RVACS is shown in Fig. 7. The lower coolant temperature initially reduced the power removed by RVACS by more than 40%, but the relative effect decreased during the transient. The lower initial coolant temperature also delayed the time when the power

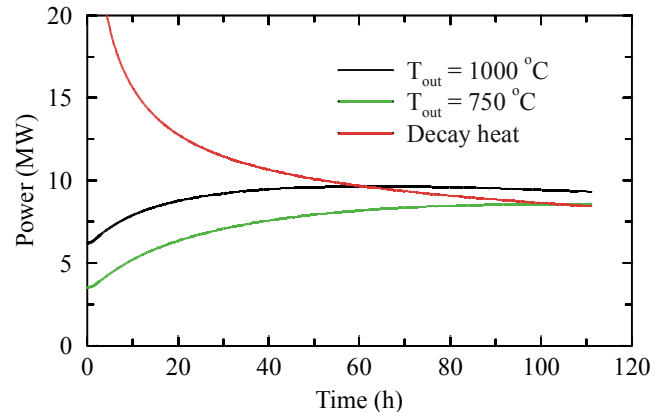removed by RVACS exceeded the core decay power by about 40 hours.

Fig. 7. The effect of initial coolant temperature on the power removed by RVACS.

The initial coolant temperature significantly affected the maximum fuel temperature following a loss of forced convection. Figure 8 shows that the lower initial coolant temperature reduced the maximum fuel temperature by 90 °C during the transient. The lower initial coolant temperature also resulted in a slower increase in fuel temperature during the transient and delayed the occurrence of the maximum fuel temperature.
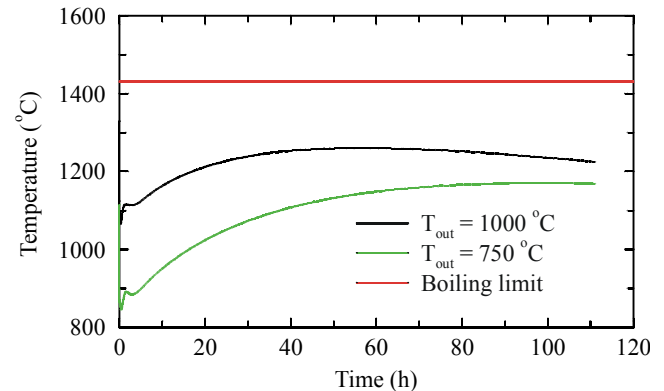

Fig. 8. The effect of initial coolant temperature on the maximum fuel temperature following a loss of forced convection.

The calculations discussed previously were based on the PRISM RVACS design. An enhanced RVACS design has been proposed for S-PRISM.[15] The enhanced RVACS design utilizes ribs to trip the boundary layer and increase the heat transfer coefficient in the riser because of thermal entry region effects. The enhanced design also includes a perforated plate in the RVACS downcomer to increase the surface area for heat transfer.

A RELAP5-3D model of the enhanced RVACS design was developed. The boundary layer trips were modeled by

increasing the heat transfer coefficient on the outer surface of the guard vessel and the inner surface of the collector cylinder by a factor of 1.6. This factor accounts for the enhanced heat transfer in the thermal entry region for a circular tube with constant heat rate[16] assuming that the ribs are effective in tripping the boundary layer. The perforated plate was modeled as an additional heat structure in the riser. The holes in the perforated plate, which were assumed to occupy 40% of the surface area, allowed the guard vessel to radiate to both the perforated plate and the collector cylinder. The gaps on either side of the perforated plate were represented as a single flow path in the model.

The enhanced design increased the power removed by RVACS by 26% at steady state. Most of the increased heat transfer was due to the ribs. The effects of the RVACS enhancements on the power removed during the transient are shown in Fig. 9. The power removed by RVACS exceeded the core decay power about 30 hours earlier with the enhanced design. The maximum fuel temperature was 87 °C lower with the enhanced design as shown in Fig. 10.
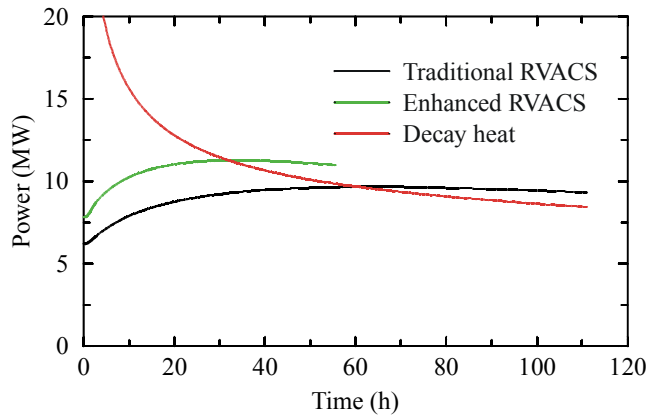

Fig. 9. The effect of design enhancements on the power removed by RVACS.
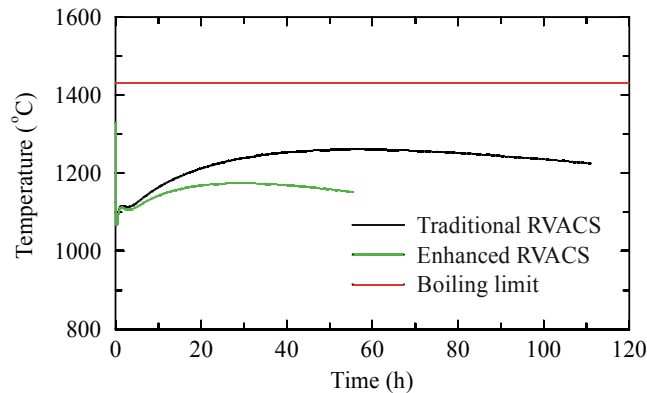

Fig. 10. The effect of RVACS design enhancements on the maximum fuel temperature following a loss of forced convection.

A parametric calculation was performed to investigate the performance of the LS-VHTR following loss of forced convection with a failure to scram. The Doppler reactivity feedback coefficient was assumed to be -0.01$/°C. The coolant density feedback coefficient was calculated from a total voiding worth of -0.03$.

The effect of the failure to scram on reactor power early in the transient is shown in Fig. 11. In the base calculation, the scram quickly reduced the power to decay heat levels. Without scram, the loss of forced circulation caused the fuel temperature to increase which caused negative reactivity feedback and slowly reduced the core power. The reactivity feedback was eventually able to shut down the reactor. The long-term power response was similar to that shown previously.
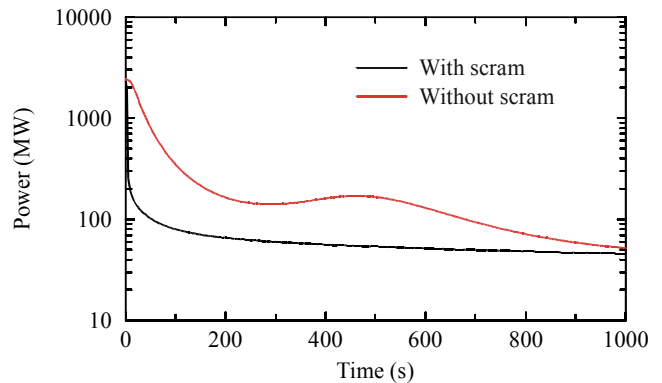

Fig. 11. The effect of a failure to scram on the reactor power following a loss of forced convection (short term).

The effect of the failure to scram on average fuel temperature early in the transient is shown in Fig. 12. The loss of forced convection coupled with a failure to scram caused the average fuel temperature to increase until reaching a peak near 90 s. The fuel temperature then decreased in response to the reduction in power caused by reactivity feedback and the establishment of natural circulation flow. However, the fuel temperature increased again in the long term because the core decay power exceeded that removed by the RVACS. Figure 13 shows that the maximum fuel temperature without scram remained above the corresponding value with scram for the duration of the transient. A long-term maximum in fuel temperature occurred near 50 hours, but this maximum was about 70 °C less than the peak value that occurred early in the transient. These results indicate the LS-VHTR can withstand a failure to scram and still remain below the boiling limit.
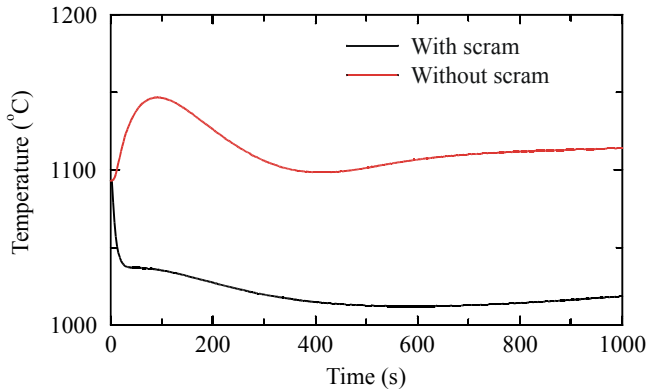
Fig. 12. The effect of a failure to scram on the average fuel temperature following a loss of forced convection (short term).
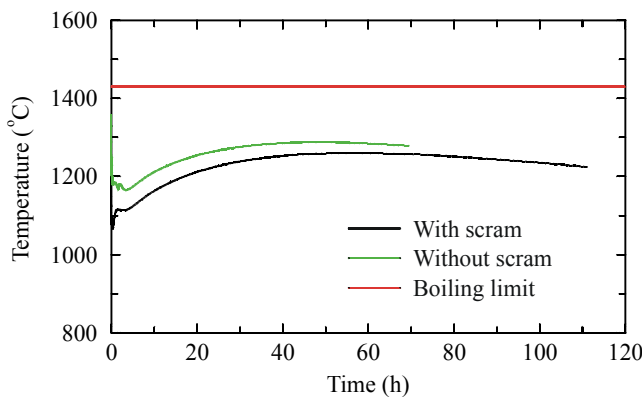

Fig. 13. The effect of a failure to scram on the maximum fuel temperature following a loss of forced convection (long term).

A final parametric calculation was performed to investigate the effects of radial and axial conduction in the core. In the base calculation, the effects of radial conduction between fuel columns and axial conduction within a fuel column were simulated using an enclosure model similar to the one developed for the NGNP. In the parametric calculation, the conduction enclosure model was deleted, leaving natural circulation of the liquid salt as the only heat transfer transport mechanism between the core and the thermal blanket system after the loss of forced convection.

The parametric calculation showed that radial and axial conduction are not important heat transport mechanisms in the LS-VHTR, a very different result from that obtained in the gas-cooled NGNP. The maximum fuel temperatures at steady state and during the transient in the parametric calculation differed by less than 1 °C from the results obtained in the base calculation. Thus, natural circulation is the dominant heat transport mechanism following loss of forced convection in the LS-VHTR.

V. CONCLUSIONS

The RELAP5-3D one-dimensional annular model accurately represents the heat conduction process in a unit cell of a fuel block. Fuel centerline temperatures calculated with the one-dimensional RELAP5-3D model were within 2.2 °C of the values obtained with a multi-dimensional ABAQUS model for a wide range of volumetric power generation rates.

The RELAP5-3D model of the LS-VHTR was used to simulate the reactor's performance during steady operation and during a transient initiated by a loss of forced convection. Steady operation at full power is more challenging than the transient with regards to temperature limits. In fact, the maximum predicted fuel temperature was about 1330 °C, which exceeds the steady state temperature limit of 1250 °C. A variety of options are available to lower the maximum fuel temperature, including lowering the operating power or fluid temperature. The maximum calculated fuel temperature during the transient was about 1260 °C and occurred about 60 hours after the loss of forced convection. The peak fuel temperature during the transient was less than the temperature during normal operation and was considerably less than the transient temperature limit of 1430 °C. Natural circulation of the liquid salt was the dominant heat transport mechanism within the reactor vessel. Transient temperature limits were met even with a failure to scram.

An RVACS model based on the PRISM design was able to adequately cool the LS-VHTR, even with a decay heat curve that was about 5% too high based on best-estimate calculations of a similar gas-cooled reactor. An enhanced RVACS model based on the S-PRISM design was also developed. The maximum fuel temperature during the transient was reduced by about 90 °C with the enhanced RVACS. However, since the temperature response during the transient is less limiting than that during normal operation, RVACS enhancements are not needed at this time. RELAP5-3D should be benchmarked against RVACS experiments to provide additional confidence in the predicted results.

The effectiveness of the RVACS during a transient in which salt leaks into the gap between the reactor and guard vessels should be evaluated further. A preliminary evaluation indicated that the performance of the RVACS would be degraded significantly if conduction through the salt is the only heat transport mechanism. Liquid salts are optically transparent and thus may allow significant radiation heat transport, but this has not been demonstrated experimentally. Experiments to determine the effectiveness of convection and radiation in small gaps

filled with liquid salt would be useful in determining the viability of the RVACS design for the LS-VHTR.

As expected, the maximum fuel temperatures are significantly affected by the coolant temperature. Lowering the operating coolant temperature by 250 °C lowered the maximum fuel temperature by 215 °C at steady state and by 90 °C during the transient.

The thermal-hydraulic performance of the LS-VHTR improved as the diameter of the coolant channels increased. Increasing the diameter of the coolant channel from 9.53 to 14.0 mm reduced the pressure drop across the core by more than 60% at steady state. The larger diameter also reduced the maximum fuel temperature by 25 °C at steady state, but had only a small effect during the transient.

ACKNOWLEDGMENTS

REFERENCES

1. D. T. INGERSOLL, K. T. Clarno, C. W. Forsberg, J. C. Gehin, R. W. Christensen, C. B. Davis, G. L. Hawkes, J. W. Sterbentz, T. K. Kim, T. A. Taiwo, and W. S. Yang, *Status of Physics and Safety Analyses for the Liquid-Salt-Cooled Very High-Temperature Reactor (LS-VHTR)*, ORNL/TM-2005/218, December 2005.

2. INEEL, *RELAP5-3D Code Manual*, Rev. 2.2, INEEL EXT-98-00834, October 2003.

3. C. B. DAVIS, T. D. Marshall, and K. D. Weaver, "Modeling the GFR with RELAP5-3D," *2005 RELAP5 International Users Seminar*, Jackson Hole, Wyoming, September 7-9, 2005.

4. P. MACDONALD, *Feasibility Study of Supercritical Light Water Cooled Reactors for Electric Power Production*, INEEL/EXT-04-02530, January 2005.

5. P. E. MACDONALD and J. Buongiorno, *Design of an Actinide Burning, Lead or Lead-Bismuth Cooled Reactor That Produces Low Cost Electricity*, INEEL/EXT-02-01249, MIT-ANP-PR-092, October 2002.

6. C. B. DAVIS, *Implementation of Molten Salt Properties into RELAP5-3D/ATHENA*, INEEL/EXT-05-02658, January 2005.

7. HIBBITT, KARLSSON & SORENSEN, Inc., ABAQUS Version 6.4-4, 2005.

8. P. E. MACDONALD et al., *NGNP Point Design – Results of the Initial Neutronics and Thermal-Hydraulic Assessments During FY-03*, INEEL/EXT-03-00970, Rev. 1, September 2003.

9. GENERAL ATOMIC, *Safety Analysis Report Use of H-451 Graphite in Fort St. Vrain Fuel Elements*, GLP-5588, December 1977.

10. AMERICAN NUCLEAR SOCIETY, *Decay Heat Power in Light Water Reactors*, ANSI/ANS-5.1, 1979.

11. A. HUNSBEDT, and P. M. Magee, "Design and Performance of the PRISM Natural Convection Decay Heat Removal System," *Proceedings of the International Topical Meeting on Safety of Next Generation Power Reactors*, Seattle Washington, May 1-5, 1988, pp. 844-851.

12. GENERAL ELECTRIC, *PRISM Preliminary Safety Information Document*, Volume II, GEFR-00793, UC-87Ta, November 1986.

13. D. T. INGERSOLL, C. W. Forsberg, L. J. Ott, D. F. Williams, J. P. Renier, D. F. Wilson, S. J. Ball, L. Reid, W. R. Corwin, G. D. Del Cul, P. F. Peterson, H. Zhao, P. S. Pickard, E. J. Parma, and M. Vernon, *Status of Preconceptual Design of the Advanced High-Temperature Reactor (AHTR)*, ORNL/TM-2004/104, May 2004.

14. J. P. HOLMAN, *Heat Transfer*, Sixth Edition, McGraw-Hill Book Company, New York, 1986.

15. C. E. BOARDMAN, A. E. Dubberly, D. G. Carroll, M. Hui, A. W. Fanning, and W. Kwant, "A Description of the S-PRISM Plant," ICONE-8168, *Proceedings of ICONE-8*, Baltimore, Maryland, April 2-6, 2000.

16. W. M. KAYES and M. E. Crawford, *Convective Heat and Mass Transfer*, Second Edition, McGraw-Hill Book Company, New York, 1980.